Chaos and the continuum limit in the gravitational N-body problem. II. Nonintegrable potentials

Ioannis V. Sideris*
Department of Astronomy, University of Florida, Gainesville, Florida 32611

Henry E. Kandrup†
Department of Astronomy, Department of Physics, and Institute for Fundamental Theory
University of Florida, Gainesville, Florida 32611
(February 25, 2002)

This paper continues a numerical investigation of the statistical properties of 'frozen-N orbits,' *i.e.*, orbits evolved in frozen, time-independent N-body realisations of smooth density distributions ρ corresponding to both integrable and nonintegrable potentials, allowing for $10^{2.5} \leq N \leq 10^{5.5}$. The focus is on distinguishing between, and quantifying, the effects of graininess on initial conditions corresponding, in the continuum limit, to regular and chaotic orbits. Ordinary Lyapunov exponents χ do not provide a useful diagnostic for distinguishing between regular and chaotic behaviour. Frozen-N orbits corresponding in the continuum limit to both regular and chaotic characteristics have large positive χ even though, for large N, the 'regular' frozen-N orbits closely resemble regular characteristics in the smooth potential. Alternatively, viewed macroscopically both 'regular' and 'chaotic' frozen-N orbits both diverge as a power law in time from smooth orbits with the same initial condition. However, convergence towards the continuum limit is much slower for chaotic orbits. For regular orbits, the time scale associated with this divergence $t_G \sim N^{1/2} t_D$, with t_D a characteristic dynamical, or crossing time; for chaotic orbits $t_G \sim (\ln N) t_D$. For $N > 10^3 - 10^4$, clear distinctions exist between phase mixing of initially localised ensembles which, in the continuum limit, exhibit regular versus chaotic behaviour. Regular ensembles evolved in a frozen-N density distribution diverge as a power law in time, albeit more rapidly than ensembles evolved in the smooth distribution. Chaotic ensembles diverge in a fashion that is roughly exponential, albeit at a larger rate than that associated with the exponential divergence of the same ensemble evolved in the smooth ρ. For both regular and chaotic ensembles, finite-N effects are well mimicked, both qualitatively and quantitatively, by energy-conserving white noise with amplitude $\eta \propto 1/N$. This suggests strongly that earlier investigations of the effects of low amplitude noise on phase space transport in smooth potentials are directly relevant to real physical systems.

PACS number(s): 05.45.-a, 05.60.-k, 51.10.+y, 98.10.+z

I. INTRODUCTION

This is the second in a series of papers, the aim of which is to understand the role of discreteness effects, *i.e.,* graininess, in the gravitational N-body problem. Particular emphasis is given to the meaning of chaos and various manifestations of chaotic behaviour. As discussed in the first paper [1] (hereafter Paper I), this problem can be divided into two separate components, namely first understanding how graininess alters the motions of representative orbits in a fixed gravitational potential and only then considering how these changes are manifested in the context of a fully self-consistent N-body evolution. As in Paper I, the focus here is on the former issue.

One is thus led naturally to effect a statistical comparison between (1) orbits evolved in a frozen N-body density distribution generated by randomly sampling some specified smooth density distribution ρ and (2) orbits evolved in the smooth potential Φ related to ρ by Poisson's equation, $\nabla^2\Phi = 4\pi G\rho$.

In this setting, the present paper has two specific objectives, namely (1) to implement precise, quantitative distinctions between 'regular' and 'chaotic' behaviour in such frozen-N systems; and (2) to determine the extent to which discreteness effects can be mimicked successfully by a suitably defined 'noise' acting on orbits evolving in an otherwise smooth potential.

Section II provides an overview of the motivations for, and scope of, this paper. Section III describes the potentials that were considered and the numerical experiments that were performed. Section IV described the results derived for individual frozen-N trajectories, determining how these results scale with N and demonstrating the extent to which they can be mimicked by a suitably defined white noise. Section V then describes the results derived for the phase mixing of orbit ensembles, again considering both how things scale with N and the degree to which discreteness effects can be mimicked by noise. Section VI focuses on the possibility of transitions between 'regular' and 'chaotic' behaviour, a phenomenon which, especially for small N, can be important for systems where the smooth potential allows a coexistence of large measures of both regular and chaotic orbits. Section VII concludes by summarising the principal conclusions and speculating on potential implications.

II. OVERVIEW

Implementing useful distinctions between regular and chaotic behaviour in frozen-N orbits is not completely trivial. For example, ordinary Lyapunov exponents computed for individual orbits do not provide a useful diagnostic. Even for density distributions corresponding to integrable potentials, N-body orbits have large positive Lyapunov exponents. Moreover, even though there is a precise sense in which, as N increases, frozen-N orbits come to more closely resemble regular orbits in the smooth potential, the values of these exponents do *not* decrease systematically with increasing N [2,1].

Viewed macroscopically, a frozen-N orbit and a smooth orbit evolved from the same initial condition in density distributions corresponding to an integrable potential will typically diverge *linearly* in time on a time scale $t_G \propto N^{1/2}$. As discussed in Paper I, this superficially surprising result would appear to reflect the fact that the chaos is associated with a large number of encounters with neighbouring particles, each of very short duration, which tend to cancel systematically so as to have a comparatively minor macroscopic effect.

Following the pioneering work of Chandrasekhar [3,4], one might anticipate that discreteness effects act in much the same way as friction and white noise, so that they can be modelled in the context of a Fokker-Planck description. To the extent that this intuition is correct, earlier work probing the effects of friction and noise on smooth potential orbits translate into specific predictions as to the expected effects of graininess.

The amplitude η associated with friction and noise defines a characteristic relaxation time $t_R = 1/\eta$ on which, *e.g.,* the perturbation will induce significant changes in conserved quantities like energy. However, modelling discreteness effects as a sequence of close binary encounters leads to the prediction [4] that $t_R \propto (N/\ln N)t_D$, with t_D a characteristic dynamical, or crossing, time. One might, therefore, anticipate that discreteness effects in a system of N bodies can be reproduced by friction and noise with amplitude $\eta \propto \ln N/N$.

When subjected to friction and white noise, regular orbits in a smooth potential typically diverge as a power law from unperturbed orbits with the same initial condition. One might, therefore, conjecture that discreteness effects will induce a power law divergence between frozen-N orbits and smooth characteristics with the same initial condition, and that the divergence time scale t_G for a system of N bodies can be mimicked by noise with amplitude $\eta \propto \ln N/N$. As noted in Paper I, frozen-N orbits and smooth regular characteristics do indeed tend to diverge linearly on a time scale $t_G \propto N^{1/2}t_D$; and, as will be seen below, this linear divergence is well reproduced by an appropriately defined white noise with amplitude $\eta \propto 1/N$. (Given the limited dynamical range in particle number for the simulations described in this paper – $10^{2.5} \le N \le 10^{5.5}$ – it would seem impossible to distinguish unambiguously between scalings $\eta \propto 1/N$ and $\eta \propto \ln N/N$. The simulations are consistent with both.)

When subjected to friction and white noise, chaotic orbits behave very differently. Comparatively weak perturbations typically induce an initial exponential divergence from the unperturbed orbit at a rate Λ that is comparable to the largest (finite time) Lyapunov exponent χ_S for the unperturbed orbits [5]. For stronger perturbations, the separation between perturbed and unperturbed orbits quickly becomes 'macroscopic,' at which point the divergence become slower than exponential, albeit still more rapid than what is observed for regular orbits. One might, therefore, expect that, when acting on chaotic initial conditions, discreteness effects associated with a finite-N system would induce (1) an initial exponential divergence at a rate Λ that is comparable to χ_S, a number typically much smaller than the 'true' Lyapunov exponent χ associated with orbits in the frozen-N system, followed by (2) a slower subexponential divergence which is still faster than the divergence associated with regular orbits.

The simulations summarised in this paper provided unambiguous confirmation of the second of these expectations. Viewed macroscopically, frozen-N orbits corresponding in the continuum limit to chaotic orbits typically diverge *linearly* from smooth orbits with the same initial condition; but for large N the time scale $t_G \propto (\ln N)t_D$ associated with this divergence is much shorter than the time scale $t_G \propto N^{1/2}t_D$ associated with regular orbits.

Unperturbed orbits in a smooth integrable potential are multiply periodic and, as such, have Fourier spectra with power concentrated at a countable set of discrete frequencies. Friction and noise destroy this exact periodicity, resulting in a more complex Fourier spectrum. To the extent that the friction and noise are weak, the orbit should remain nearly regular and the spectrum should remain 'similar to' the spectrum associated with the unperturbed orbit. However, when the friction and noise become larger in amplitude the orbit should become 'less nearly periodic,' and the spectrum should become 'more complex' than the spectrum associated with the unperturbed orbit. In the same sense, one might expect that, as N decreases, frozen-N orbits corresponding to regular orbits in a smooth potential will become 'less regular' and be characterised by Fourier spectra that are 'more complex'. This intuition can be made precise by computing from an orbital time series such quantifiable measures of orbital complexity [6] as (1) the number of frequencies in a discrete Fourier series that contain more than some fixed fraction j of the power in the peak frequency or (2) the minimum number of frequencies required to capture a fixed fraction k of the total power.

By contrast, chaotic orbits in a smooth potential are in general aperiodic [7]. This implies that, even in a discrete time series, their power should be spread over a larger number of frequencies, so that the orbit will have substantially larger 'complexity' [6]. For very small N, where the qualitative character of the orbits is dominated by close encounters and distinctions between chaotic and regular motions are difficult to identify, one might expect that frozen-N orbits corresponding in the continuum limit to regular and chaotic orbits would have comparable complexities, much larger than the typical complexity associated with a smooth regular orbit and larger even than the complexity associated with a smooth chaotic orbit. As N increases, discreteness effects will presumably become less important and the complexity of both the regular and chaotic frozen-N orbits will decrease. For the case of regular frozen-N orbits, the complexity should eventually converge towards the comparatively small value associated with a smooth regular orbit. For the case of chaotic frozen-N orbits, the complexity should instead converge towards the substantially larger value associated with a smooth chaotic orbit.

To the extent that discreteness effects associated with a fixed number N can be successfully modelled in terms of a suitably defined noise with amplitude η, one might also expect that the typical complexity $n(N)$ associated with a frozen-N orbit with given N will be comparable to the complexity $n(\eta)$ associated with a smooth orbit with the same initial condition evolved in the presence of perturbations of amplitude $\eta \propto 1/N$.

As described below, both these intuitions were in fact confirmed.

Discreteness effects can also be explored in the context of the phase mixing of initially localised orbit ensembles, a subject which has received considerable attention in both galactic astronomy [8–10] and accelerator dynamics [11,12] since Merritt and Valluri [13] coined the term 'chaotic mixing' to characterise the much more efficient phase mixing associated with ensembles of chaotic orbits.

Localised ensembles of regular initial conditions evolved in a smooth potential will initially diverge as a power law in time and, when viewed over much longer time scales, exhibit a coarse-grained evolution, again proceeding as a power law in time, towards a time-independent equilibrium state. The introduction of friction and noise accelerates the original divergence, but that divergence still proceeds as a power law in time. Quantifying the later time evolution is more subtle because the perturbations allow the orbits to access phase space regions which would otherwise be inaccessible. However, what *is* clear is that, as probed by various lower order moments, the ensemble evolves exponentially in time towards a 'well-mixed' state that manifests the symmetries of the unperturbed potential. If, *e.g.,* the potential admits a reflection symmetry, $\Phi(-x) = \Phi(x)$, the mean value $\langle x \rangle$ associated with the ensemble will converge exponentially towards zero.

By contrast, localised ensembles of chaotic orbits evolved in a smooth potential initially diverge exponentially at a rate Λ that is comparable to the value of the largest Lyapunov exponent χ_S and, when viewed over somewhat longer time scales, exhibit a coarse-grained evolution, exponential in time, towards a time-independent, or nearly time-independent state. The rate λ associated with this subsequent evolution is typically much smaller than Λ and is not directly related to χ_S, although loose correlations between λ and χ_S often exist [13]. Subjecting these same ensembles to friction and noise typically increases the rate Λ associated with the initial divergence, making the orbits behave in a fashion that is 'even more chaotic.' Over sufficiently long time scales, these perturbations will drive the ensemble towards a thermal state with a temperature Θ set by the friction and noise. However, on time scales much shorter than the natural time scale t_R associated with the friction and noise, the ensemble will again evolve towards a nearly time-independent distribution; and, in many cases, the perturbations will increase the rate λ associated with this convergence towards a near-equilibrium. [18].

The simulations described here demonstrate that, both qualitatively and quantitatively, discreteness effects impact phase mixing for both regular and chaotic orbits in much the same way as these perturbations.

Perhaps the most important conclusion of the work described here is the apparent need to distinguish between two distinct 'types' of chaos. Short-range *microscopic chaos* associated with close encounters between individual masses, is a ubiquitous phenomenon for the N-body problem, which appears to be present irrespective of the bulk properties of the density distribution. In addition, however, there is the possibility of *macroscopic chaos*, easily identified in the continuum limit, which has predictable implications for motions in the N-body problem.

III. DESCRIPTION OF THE NUMERICAL EXPERIMENTS

The numerical experiments described here focused on orbits and orbit ensembles evolved in frozen-N realisations of four different time-independent density distributions. In the continuum limit, two of these correspond to integrable potentials; the other two correspond to potentials which admit large measures of chaos. These orbits and orbit ensembles were also compared with orbits with the same initial conditions evolved in the smooth potentials associated with the smooth density distributions, both with and without noise. Each system was normalised to have mass $M = 1$, and units were so chosen that the gravitational constant $G = 1$. The four density distributions were the following:

1. A spherically symmetric Plummer sphere, for which

$$\rho_P(r) = \left(\frac{3M}{4\pi b^3}\right)\left(1+\frac{r^2}{b^2}\right)^{-5/2}. \tag{3.1}$$

This corresponds via Poisson's equation to a potential

$$\Phi_P(r) = -\frac{GM}{\sqrt{r^2+b^2}}. \tag{3.2}$$

Units were chosen such that $b = 1$.

2. A constant density triaxial ellipsoid, for which

$$\rho_E(\mathbf{r}) = \frac{3M}{4\pi abc} \times \begin{cases} m^2 & \text{if } m^2 \le 1, \\ 0 & \text{if } m^2 > 1, \end{cases} \tag{3.3}$$

with

$$m^2 = \left(\frac{x^2}{a^2} + \frac{y^2}{b^2} + \frac{z^2}{c^2} \right). \tag{3.4}$$

For $m \le 1$, this yields a potential of the form

$$\Phi_E(\mathbf{r}) = \Phi_0 + \frac{1}{2}\left(\omega_a^2 x^2 + \omega_b^2 y^2 + \omega_c^2 z^2\right) \tag{3.5}$$

with frequencies ω_a, ω_b, ω_c, related to the axis values a, b, c, in terms of incomplete elliptic integrals [14]. Attention focused primarily on the specific parameter values $a = 1.95$, $b = 1.50$, and $c = 1.05$, which imply $\Phi_0 \approx -1.00608$, $\omega_a \approx 0.4663$, $\omega_b \approx 0.5508$, and $\omega_c \approx 0.6753$.

3. A constant density ellipsoid perturbed by a supermassive black hole, corresponding to the potential

$$\Phi_{BH} = \Phi_E - \frac{GM_{BH}}{\sqrt{r^2 + \epsilon^2}}, \tag{3.6}$$

with $\epsilon = 10^{-3}$. Attention here focused on a black hole mass $M_{BH} = 10^{-1.5} M \approx 0.0316228 M$. This yields [15] a potential for which, for orbits restricted energetically to $m \le 1$, the phase space is almost completely chaotic.

4. A triaxial generalisation of the Dehnen [16] potential, for which

$$\rho_D(\mathbf{r}) = \frac{M(3-\gamma)}{4\pi abc} m^{-\gamma} (1+m)^{-(4-\gamma)}, \tag{3.7}$$

with m again given by eq. (3.4). Attention focused on the parameter values $\gamma = 1$ and $a = 1.0$, $b = \sqrt{5.0/8.0}$, and $c = 0.5$, values first considered by Merritt and Fridman [17] as a prototype for a cuspy triaxial galaxy. The phase space associated with this potential has been studied extensively [17,18] and it is known that, especially for low energies, there exist large measures of both regular and chaotic orbits. The smooth potential Φ_D associated with ρ_D cannot be written analytically, so that integrations in Φ_D were performed using a 32nd order Gauss-Legendre integration scheme written by C. Siopis as part of his Ph. D. dissertation [19].

Independent of energy, the characteristical orbital time scale for motion in the constant density ellipsoid, with or without a black hole, corresponds to a dynamical time $t_D \sim 10$. (The quantity $1/\sqrt{G\rho} \approx 3.6$.) The experiments with the Plummer potential described in this paper were performed for intermediate energies for which, again, $t_D \sim 10$. The Dehnen potential exhibits a much larger degree of central concentration and, as such, t_D exhibits greater variability.

The ellipsoid potential (3.3) is particularly simple in the sense that, in the continuum limit, all orbits oscillate with the same periodicities so that there is *no phase mixing*. Any phase mixing observed in a frozen-N simulation must be attributed to discreteness effects. Given, moreover, that the statistical properties of noisy orbits in a harmonic potential are well understood, it is comparatively simple to determine whether these discreteness effects can be well represented by noise. The Plummer potential is more realistic in that the orbits oscillate with different periodicities so that, even in the continuum limit, phase mixing occurs.

The nonintegrable potential (3.6) is simple in the sense that, for the energies and black hole masses considered here, almost all smooth orbits are chaotic. This implies that, when considering N-body realisations, one need not be much concerned about the possibility of graininess converting an initially 'chaotic' orbit into a 'regular' orbit. By contrast, the smooth Dehnen potential admits large measures of both regular and chaotic orbits, so that graininess could well induce numerous transitions between 'regular' and 'chaotic' behaviour.

Frozen-N density distributions of the form

$$\rho_N = \frac{1}{N} \sum_{i=1}^{N} \delta_D(\mathbf{r} - \mathbf{r}_i) \tag{3.8}$$

were generated by randomly sampling the smooth density distributions ρ. These correspond to N-body potentials

$$\Phi_N(\mathbf{r}) = -\frac{1}{N} \sum_{i=1}^{N} \frac{1}{\sqrt{(\mathbf{r} - \mathbf{r}_i)^2 + \epsilon^2}} \tag{3.9}$$

which incorporate a tiny 'softening parameter' with value $\epsilon \le 10^{-3}$.

Orbits were integrated in frozen-N realisations with $10^{2.5} \le N \le 10^{5.5}$. The integrations were performed with a variable time step integration scheme which was guaranteed to conserve the energy of each particle to at least one part in 10^3. The energy of a typical orbit was conserved to within a few parts in 10^5. Estimates of the largest (finite time) Lyapunov exponents orbits were obtained in the usual way by simultaneously tracking the evolution of a small initial perturbation, periodically renormalised at fixed intervals Δt [20]. The finite time Lyapunov exponents derived in this fashion typically exhibited rapid convergence towards near-constant values – much more rapid convergence than has been observed [15,18] for the smooth potentials – so that a time ~ 100 dynamical, or crossing, times t_D was sufficient to yield reasonable estimates.

Some of the orbital data were Fourier analysed to determine their 'orbital complexity' [6]. This entailed determining for each orbit the quantities n_x, n_y, and n_z, defined, respectively, as the minimum number of frequencies required to capture a fixed fraction k of the power in each direction, and then assigning a total complexity

$$n = n_x + n_y + n_z. \tag{3.10}$$

In order to obtain a reasonably sharp Fourier spectrum, orbital data were typically recorded at intervals

$\delta t = 0.01 t_D$ or less, and each orbit was represented by a time series containing at least 4096 points.

Phase mixing in frozen-N systems was explored by performing integrations of orbit ensembles comprised (mostly) of 1600 initial conditions localised within a phase space hypercube of size $\sim 10^{-3}$ the size of the accessible phase space region. For each cell of initial conditions, experiments were typically repeated for several different frozen-N density distributions, each sampling the same smooth ρ, so as to extract improved statistics. The experiments with $N = 10^{2.5}$, 10^3 and $10^{3.5}$ were each performed for six different frozen-N density distributions, those with $N = 10^4$ and $10^{4.5}$ for four distributions, and those for $N = 10^5$ for two distributions. Because of computational constraints – each orbit with $N = 10^{5.5}$ averaged roughly three hours on a Pentium 200 workstation –, the long time ensemble integrations for $N = 10^{5.5}$ were performed for only one ensemble, comprised of 800, rather than 1600, orbits. However, the first fifth of each integration, in many respects the most interesting, *was* repeated for a second frozen-N distribution.

To test the intuition that discreteness effects can be mimicked by friction and white noise in the context of a Fokker-Planck description, orbit ensembles were also evolved in the smooth potential in the presence of a suitably defined 'white noise.' Ordinarily, discreteness effects are modeled by considering a Langevin equation [21]

$$\frac{d^2 r_a}{dt^2} = -\nabla_a \Phi - \eta \frac{dr_a}{dt} + F_a, \qquad a = x, y, z. \qquad (3.11)$$

Here $\eta dr_a/dt$ represents a dynamical friction and F_a represents Gaussian white noise, which is characterised completely by its first two moments:

$$\langle F_a(t) \rangle = 0, \qquad (a, b = x, y, z)$$

and

$$\langle F_a(t_1) F_b(t_2) \rangle = 2\eta \Theta \delta_{ab} \delta_D(t_1 - t_2), \qquad (3.12)$$

where $D \equiv 2\eta\Theta$ represents the diffusion constant entering into a Fokker-Planck description. Choosing Θ to equal the initial energy then ensures that the average energy of the orbits remains unchanged.

Such an equation is unsatisfactory here. Energy is conserved absolutely for frozen-N orbits, so that one must also impose energy conservation on any scheme which aims to mimic its effects. (For very small η, energy remains almost conserved for very long times. However, comparatively small N should correspond to relatively large η, which implies large changes in energy and, as such, significant changes in the phase space regions accessible to the noisy orbit.) For this reason, the noisy integrations described here were performed using a modified energy-conserving noise.

This entailed (1) eliminating the dynamical friction altogether, (2) again imparting random kicks as in eq. (3.12), but (3) renormalising the modified velocity at each time step by an overall factor, *i.e.*, $\mathbf{v}(t + \delta t) \rightarrow \alpha \mathbf{v}(t + \delta t)$, with α so chosen that $E(t + \delta t) = E(t)$. Modulo this complication, the noise was integrated using a standard algorithm [22] based on a fourth order Runge-Kutta integration scheme with fixed time step δt. The integrations were performed for $\delta t = 2 \times 10^{-4}$, it having been confirmed that the statistical effects of the noise were insensitive to the precise value of δt for $\delta t < 10^{-3}$.

IV. 'REGULAR' AND 'CHAOTIC' ORBITS

A. Ordinary Lyapunov exponents a useless diagnostic for macroscopic chaos

In terms of Lyapunov exponents for individual orbits, it appears impossible to distinguish between frozen-N trajectories corresponding to regular orbits in a smooth potential and frozen-N trajectories corresponding to chaotic orbits. 'Regular' and 'chaotic' frozen-N orbits have positive Lyapunov exponents which are comparable in magnitude, and that magnitude is typically much larger than the magnitude of the largest Lyapunov exponent for chaotic orbits evolved in the smooth potential.

This is illustrated by Fig. 1, which exhibits, as functions of N, estimates of the largest Lyapunov exponents for frozen-N realisations of the homogeneous ellipsoid, both with and without a central mass. Each curve in this Figure represents a mean value extracted by averaging over four different initial conditions. The three curves correspond to regular initial conditions evolved in an ellipsoid with $M_{BH} = 0$ (solid line) and 'sticky chaotic' (dashed lines) and 'wildly chaotic' (dot-dashed lines) initial conditions evolved in an ellipsoid with $M_{BH} = 10^{-1.5}$. (Recall [23] that 'sticky chaotic' orbit segments correspond to segments of a chaotic orbit which are confined temporarily near a regular island and behave in a nearly regular fashion.) Three points are immediately apparent: (1) The estimates of χ computed for these three different sets of initial conditions are very nearly equal in magnitude. (2) Consistent with the results described in Paper I, one observes no systematic dependence on N. (3) The typical value of χ is comparatively large, much larger than the typical values χ_S associated with motion in the smooth potential. For the values of energy E and mass M_{BH} used to generate these χ's, 'wildly chaotic' orbit segments in the smooth potential typically have $\chi_S \sim 0.055$ and 'sticky' segments have $\chi_S \sim 0.022$.

That 'regular' orbits with $M_{BH} = 0$ and 'chaotic' orbits with $M_{BH} > 0$ have χ's that are approximately equal, and that this value is much larger than χ_S, suggests strongly that these exponents reflect almost completely the effects of 'microscopic' chaos associated with close encounters, and that the form of the bulk potential is largely immaterial. In both cases the frozen-N orbits are moving through an ellipsoid with the same constant density; and, since the black hole mass $M_{BH} =$

$10^{-1.5} \ll 1$, the presence or absence of the black hole does not significantly impact the natural orbital time scale.

B. The divergence of N-body orbits from smooth characteristics

One way to effect macroscopic comparisons of frozen-N orbits and smooth characteristics generated from the same initial condition is by computing such diagnostics as the configuration and velocity space separations,

$$Dr(t) \equiv |\mathbf{r}_S(t) - \mathbf{r}_N(t)| \qquad \text{and}$$
$$Dv(t) \equiv |\mathbf{v}_S(t) - \mathbf{v}_N(t)|, \tag{4.1}$$

where $(\mathbf{r}_S, \mathbf{v}_S)$ and $(\mathbf{r}_N, \mathbf{v}_N)$ denote, respectively, phase space coordinates for orbits in the smooth and frozen-N density distributions.

It was found in Paper I that, for individual regular orbits [25], Dr and Dv typically grow linearly in time. A corresponding analysis for chaotic orbits is somewhat less conclusive since, apparently, different chaotic orbits can exhibit a larger degree of variety in their behaviour. However, by averaging over an ensemble of m different initial conditions, and computing the mean separation

$$\mathcal{D}r(t) \equiv \frac{1}{n}\sum_{i=1}^{m} Dr_i(t), \tag{4.2}$$

and an analogous $\mathcal{D}v(t)$, one can again extract an unambiguous trend. As for the case of regular orbits, so also for chaotic orbits, viewed macroscopically *$\mathcal{D}r$ and $\mathcal{D}v$ diverge linearly in time.* This is, *e.g.*, illustrated in the first seven panels of Fig. 2, which was generated by effecting pointwise comparisons of 800 smooth and frozen-N orbits in the potential (3.6) for different values of N ranging between $N = 10^{2.5}$ and $N = 10^{5.5}$. The initial conditions, chosen identically for each value of N, were selected so as to correspond to 'wildly chaotic' orbits, for which a typical finite time Lyapunov exponent $\chi_S \approx 0.055$.

'Regular' and 'chaotic' frozen-N orbits are similar in that they both diverge from a smooth characteristic with the same initial condition as a power law in time: $\mathcal{D}r = A_G t$. However, the characteristic time scales involved are very different. For regular orbits in the Plummer potential, it was found (*cf.* eq. (4.8) in Paper I) that

$$t_G \approx A_{G,reg} N^{1/2} t_D, \qquad \text{regular} \tag{4.3}$$

where t_D a characteristic crossing time and $A_{G,reg}$ is a constant of order unity. For chaotic orbits in the Dehnen potential and the ellipsoid plus black hole potential (3.6), one discovers instead that

$$t_G \approx A_{G,cha} (\ln N) t_D, \qquad \text{chaotic} \tag{4.4}$$

where, again, $A_{G,cha}$ is of order unity.

The goodness of fit to such a logarithmic dependence is exhibited in the final panel of Fig. 2, which exhibits growth times t_G derived from least squares fits to the data in the preceding panels. This panel should be contrasted with Fig. 8 in Paper I, which exhibits an analogous curve derived for regular orbits in the Plummer potential.

C. Distinctions based on orbital 'complexity'

The fact that, as N increases, frozen-N orbits remain close to smooth characteristics with the same initial condition for progressively longer times implies that, in terms of visual appearance, they also tend to more closely resemble those smooth characteristics. This visual impression is easily corroborated by an examination of the complexity of the Fourier spectra, which characterise the extent to which the orbits are, or are not, nearly periodic. For comparatively small N, frozen-N orbits corresponding to both regular and chaotic characteristics both look strongly aperiodic and 'wildly chaotic' in appearance. Not surprisingly, therefore, their complexities are very large, large compared even with the complexities associated with ordinary 'wildly chaotic' orbits evolved in the corresponding smooth potential. However, as N increases, the complexities of regular and chaotic frozen-N orbits both decrease and, for sufficiently large N, the complexities $n(N)$ converge towards the values n_S associated with orbits in the smooth potential. For frozen-N orbits corresponding to regular characteristics, this n_S is typically quite small; for orbits corresponding to chaotic characteristics, n_S is typically much larger.

Analogous results obtain for orbits evolved in the presence of ordinary friction and noise [26] and, as such, it is natural to ask whether the observed variations in complexity resulting from changes in N can also be mimicked by the energy-conserving noise considered in this paper. Overall, the answer to this would seem to be: yes.

Fig. 3 exhibits the mean complexity n for representative samples of orbits evolved in the potentials (3.2), (3.5), and (3.6). In each case, the complexities were computed from an orbital time series that sampled an orbit of duration $T = 512$ at intervals $\Delta t = 0.05$. The first two panels were generated for the Plummer and homogeneous ellipsoid potentials, both corresponding in the continuum limit to completely integrable motion. The last two panels exhibit complexities computed for initial conditions corresponding to 'wildly chaotic' and 'sticky chaotic' orbits in the ellipsoid plus black hole potential. In each panel, the diamonds reflect complexities computed for frozen-N orbits with different values of N and the horizontal dashed line corresponds to the mean complexity for unperturbed orbits with the same initial conditions evolved in the corresponding smooth potential. The triangles reflect complexities computed for motion in the smooth potential perturbed by noise with $\Theta = 1.0$ and a coefficient η related to N via a relation $\log_{10}\eta = \mathcal{A} - \log_{10} N$.

The constants $\mathcal{A}$ were *not* determined by using a least squares algorithm to make the two curves coincide, at least approximately. Rather, as described in Section V, the connection between η and N was effected by demanding that, for the case of regular orbits, noise of amplitude η and discreteness effects associated with a system of N particles yield phase mixing at the same rates. For the Plummer potential, this requires $\mathcal{A}_{Plum} \approx 0.0$. For the homogeneous ellipsoid, $\mathcal{A}_{ellip} \approx 0.5$. Because the black hole mass in the potential (3.6) is much smaller than the total mass of the system – $M_{BH} = 10^{-1.5}M$ – it should have only a minimal effect on the characteristic orbital time scales; and, for this reason, the last two panels involved fits assuming $\mathcal{A} = \mathcal{A}_{ellip}$.

The correspondence between frozen-N and noisy complexities is quite good, except for very small N and very large η where systematic discrepancies can be seen to occur. This means that if the amplitude of the noise is tuned so as to reproduce the expected macroscopic behaviour associated with regular phase mixing of orbit ensembles, individual noisy orbits – both regular and chaotic – will also manifest a degree of complexity comparable to that manifested by individual frozen-N orbits.

V. PHASE MIXING OF ORBIT ENSEMBLES

A. Divergence of initially localised ensembles

For particle number $N < 10^3$ or so, initially localised 'regular' and 'chaotic' ensembles both phase mix extremely rapidly in a fashion that makes it virtually impossible to distinguish between them. Inded, it would appear that, for such small N, mixing is dominated by discreteness effects and the form of the bulk potential is comparatively unimportant. However, for $N > 10^{3.5}$ or so, it becomes possible to make clean distinctions between the phase mixing of ensembles which correspond in the continuum limit to regular vis-a-vis chaotic orbits. It is, for example, evident that 'regular' ensembles disperse as a power law in time, whereas 'chaotic' ensembles disperse in a fashion that is roughly exponential.

Consider, *e.g.,* the configuration dispersion σ_r associated with an ensemble,

$$\sigma_r^2 \equiv \langle r^2\rangle - \langle r\rangle^2, \tag{5.1}$$

with

$$\langle r^p\rangle = \frac{1}{m}\sum_{i=1}^{m}(x_i^2+y_i^2+z_i^2)^{p/2}. \tag{5.2}$$

For a homogeneous ellipsoid with $M_{BH} = 0$, which corresponds in the continuum limit to integrable orbits all oscillating with the same natural frequencies, there is no phase mixing in the smooth potential, so that σ_r exhibits no systematic growth. If, however, the smooth potential is replaced by a frozen-N potential, one discovers instead that σ_r grows as $t^{1/2}$. More precisely, the growth of the dispersion is well fit by a simple relation of the form

$$\sigma_r = (t/t_G)^{1/2}, \tag{5.3}$$

where

$$t_G(N) = ANt_D \tag{5.4}$$

and A is a constant of order unity. That σ_r scales as $t^{1/2}$ is illustrated in Fig. 4, which plots $\sigma_r^2(t)$ for a single ensemble of initial conditions evolved in different frozen-N backgrounds with N varying between $N = 10^{2.5}$ and $N = 10^5$. The dots represent raw data recorded at intervals $\Delta t = 0.25$; the solid curves represent the result of 'box-car' averaging over 20 adjacent data points. In each case it is apparent that σ_r^2 exhibits a roughly linear growth until it saturates at a value ~ 0.06, this corresponding to $\sigma_r \sim 0.25$.

This $t^{1/2}$ behaviour is hardly surprising, corresponding as it does to the analytically predicted behaviour of an ensemble of 'noisy' orbits all evolved in a harmonic potential with the same natural frequencies (*cf.* [3]). That t_G exhibits a roughly linear dependence on N is consistent with the expectation [4] that discreteness effects should be manifested on a relaxation time $t_R \propto N/\ln N$. The validity of the scaling $t_G \propto N$ is illustrated in Fig. 6, which will be discussed more carefully below.

For more generic models like the Plummer potential, where different integrable orbits oscillate with different frequencies, the behaviour is more complex: For smaller N the dispersion still grows as $t^{1/2}$ on a time scale consistent with eq. (5.4), but for larger N the growth is essentially linear. This can be interpreted as arising from a competition between two effects. Regular phase mixing, present even in the continuum limit, results in a dispersion that grows linearly in time; whereas an additional 'noise-induced phase mixing' typically induces a $t^{1/2}$ divergence between perturbed and unperturbed orbits. For large N, discreteness effects have only a small effect on the phase mixing, so that the frozen-N σ_r exhibits the same linear dependence on time as the smooth potential σ_r. For smaller N discreteness effects become more important and induce a larger amplitude $t^{1/2}$ growth.

This behaviour is illustrated in the left hand panel of Fig. 5, which exhibits σ_r for evolution in the smooth Plummer potential and for frozen-N evolution with $10^{2.5} \leq N \leq 10^5$. It is evident that, for $N \geq 10^4$, the overall growth is linear, at least until the dispersion 'saturates' at a value $\sigma_r \sim 0.4$, and that this linear evolution is nearly indistinguishable from the smooth evolution. The only obvious difference is that discreteness effects tend to 'fuzz out' the systematic oscillations associated with strictly periodic orbits in the unperturbed potential which yield the large 'spread' in values of σ_r superimposed on the overall linear growth. For smaller N, $\sigma_r(t)$ is better represented by a $t^{1/2}$ growth law; and, quite apparently, the 'spread' in σ_r is substantially reduced. This reduction is a manifestation of the fact that, for smaller

N, the orbits in the ensemble exhibit significant deviations from periodicity, a fact manifested by the increased complexities discussed in the preceding Section.

Implicit in the preceding is the assumption that discreteness effects really can be mimicked by noise. This was tested at two levels, namely (i) a qualitative, visual comparison of plots of $\sigma_r(t)$ generated for both frozen-N and noisy ensembles, and (ii) a quantitative comparison of slopes associated with a $\sigma_r^2 = t/t_G$ growth law. The degree to which noise can mimic discrete effects is evident visually from a comparison of the left hand panel in Fig. 5, which was generated from frozen-N ensembles evolved in the Plummer potential, with the right hand panel, which were generated from the same ensembles of initial conditions, now evolved in the smooth potential in the presence of energy-conserving white noise. For particle number as small as $N = 10^{2.5}$, the correspondence is comparatively poor, the frozen-N σ_r growing considerably more rapidly than the noisy σ_r. However, already for $N = 10^3$ the correspondence is quite reasonble and, for $N \geq 10^4$, the frozen-N and noisy plots are essentially indistinguishable.

The preceding comparison of frozen-N ensembles with fixed N and noisy ensembles evolved with $\eta \propto 1/N$ was motivated by the fact that, at least for comparatively large η, the noisy dispersions were also well fit by a $t^{1/2}$ growth law where, however,

$$t_G = Bt_D/\eta, \qquad (5.5)$$

with B a constant of order unity. A comparison of eqs. (5.4) and (5.5) implies a natural identification

$$\log_{10}\eta = \mathcal{A} - \log_{10} N, \qquad (5.6)$$

with $\mathcal{A}$ yet another constant. For the ellipsoid potential, the best fit $\mathcal{A} = 0.0\pm0.1$. For the Plummer potential $\mathcal{A} = 0.6\pm0.1$. The identification between Figs. 5a and b assumed $\mathcal{A} = 0.5$. The extent to which the growth rates for frozen-N and noisy orbits can be related by (5.6) may be gauged from Fig. 6, which superimposes plots of $t_G(N)$ and $t_G(\eta)$ for the Plummer and ellipsoid potentials, with N and η related by eq. (5.6).

The behaviour exhibited by ensembles corresponding to chaotic orbits is very different. In this case, the dispersion associated with an ensemble evolved in the smooth potential typically diverges exponentially in time, and discreteness effects only serve to accelerate this growth. This is, *e.g.,* evident from Fig. 7a, which plots $\ln\sigma_r$ for an ensemble of initial conditions evolved in the potential (3.6) that corresponds in the continuum limit to 'wildly chaotic' orbits. It is apparent that the growth of σ_r is not strictly exponential, but it certainly *is* faster than the exponential growth associated with the smooth potential, which is exhibited in the final panel. One other point is also evident: For the case of the Plummer potential, a frozen-N integration with N as small as $N \sim 10^{4.5}$ yields phase mixing almost identical to that observed in the smooth potential. For the case of the chaotic ensemble evolved in the potential (3.6), even $N = 10^{5.5}$ yielded phase mixing that was *much more rapid* than that associated with the corresponding smooth potential.

Fig. 8a exhibits an analogous plot, again generated for the potential (3.6), but now considering an ensemble of initial conditions which, in the continuum limit, correspond to comparatively 'sticky' chaotic orbits which initially disperse much more slowly. (The typical value of the largest finite time Lyapunov exponent for smooth orbits in this 'sticky' ensemble was $\chi(t = 256) \sim 0.022$. The typical value for the 'wildly chaotic' ensemble was $\chi \sim 0.055$.) For $N \leq 10^4$ or so, Figs. 7a and 8a are comparatively similar, the 'stickiness' manifested in the continuum limit being largely lost. However, for larger N more conspicuous differences become apparent. It is, for example, clear that, for particle number as large as $N = 10^{5.5}$, the dispersion for the 'sticky' ensemble only becomes 'macroscopic' on a time scale appreciably longer than the time scale for the 'wildly chaotic' ensemble.

To a considerable degree, the behaviour exhibited by chaotic frozen-N ensembles is again well-mimicked by energy-conserving noise. This is, *e.g.,* evident from Figs.7b and 8b which, respectively, exhibit the same ensembles of initial conditions as Figs. 7a and 8a, now evolved in the smooth potential in the presence of energy-conserving white noise. The lower seven curves in these panels each involved the same identification between N and η as did Fig. 6, this motivated by the recognition that the black hole mass $M_{BH} = 10^{-1.5}$ is too small to significantly alter the natural time scale t_D. The top curve in each panel exhibits $\ln\sigma_r$ for $\eta = 10^{-7.5}$, the largest value of η that does *not* result in phase mixing that is significantly more rapid than that associated with the unperturbed smooth potential. Presuming that the correspondence between N and η established here can be extrapolated to larger N and smaller η, it follows that, for the ensembles considered here, one would require particle number as large as $N \sim 10^8$ before discreteness effects become unimportant over the time scales of interest!

One important issue is the extent to which the behaviour of orbit ensembles evolved in different frozen-N realisations of the same potential with the same number N is, or is not, the same. For the integrable Plummer and ellipsoid potentials, it would appear that, even for numbers as small as $N \sim 10^3$, the statistical properties of orbit ensembles are essentially the same for different frozen-N realisations. This, however, is *not* true for chaotic ensembles. In this case, one appears to require $N > 10^5$ or so before noticeable differences between different realisations are suppressed. This is, *e.g.,* evident in Fig. 9, which exhibits σ_r for the same initial conditions used to generate Fig. 8, now focusing on a time interval only one fifth as long and including with dotted lines the results of the different realisations which were averaged to yield the solid line.

B. Approach towards a 'well-mixed' state

That initially localised ensembles of chaotic orbits evolved in a smooth potential should diverge exponentially is more or less obvious; and the simulations described in this paper show that graininess associated with finite N has the same qualitative effect as noise with characteristic amplitude $\eta \propto 1/N$. Frozen-N evolution results in a divergence which is even faster than that associated with the unperturbed ensemble, albeit no longer strictly exponential.

Less obvious, but also true, is the fact that chaotic ensembles integrated in a smooth potential tend to evolve towards a near-equilibrium state, and that this evolution typically proceeds exponentially in time. For systems manifesting the reflection symmetries associated with the potentials explored in this paper, this implies in particular that quantities like the mean values $\langle x \rangle$ and $\langle v_x \rangle$ tend to zero exponentially. The obvious question then is whether discreteness effects, which can significantly accelerate the initial rate at which ensembles disperse, also act to accelerate the rate at which ensembles evolve towards a near-equilibrium.

Similarly, one can consider the effects of graininess on regular orbits. Unperturbed regular orbits evolved in a smooth potential do *not* exhibit a rapid exponential approach towards a (near-)equilibrium corresponding to a finite phase space volume. Rather, what one observes is a more modest power law evolution towards a near-uniform population of the invariant tori to which they are restricted. Allowing for discreteness effects allows the orbits to escape from these invariant tori and, as such, one might again ask: is there an approach towards some more general 'near-equilibrium'? And, if so, how does this approach proceed in time?

For potentials which, in the continuum limit, correspond to integrable systems, 'weak' discreteness effects associated with comparative large N have only a minimal effect on such quantities as $\langle x \rangle$. However, for smaller N systems, where discreteness effects become more important, these moments *do* converge exponentially towards zero. This is, *e.g.,* illustrated in Fig. 10a, which exhibits the quantity $\ln |\langle z \rangle|$ for frozen-N ensembles evolved in the integrable Plummer potential. Fig. 10b exhibits the same quantity computed for the same set of initial conditions, but now evolved in the smooth potential in the presence of energy-conserving noise. It is evident that, at least for comparatively large N and small η, the curves are again extremely similar. That the convergence towards $\langle z \rangle = 0$ terminates at $\ln |\langle z \rangle| \sim -3$ is a finite sampling effect, reflecting the fact that the ensembles were comprised of only 1600 orbits. Even if one were to select 'at random' 1600 points from a continuous distribution with $\langle z \rangle = 0$, one would have a sample for which $\langle z \rangle \neq 0$.

For the case of chaotic potentials one observes an exponential decrease in such moments, even in the continuum limit, but discreteness effects again serve to increase the rate associated with this evolution. This is, *e.g.,* illustrated in Figs. 11a and 12a, which exhibit $\ln |\langle z \rangle|$ for the 'wildly chaotic' and 'sticky' ensembles used to generate Figs. 7 and 8. The degree to which this enhanced exponential evolution can be mimicked by energy-conserving noise is illustrated in Figs. 11b and 12b. As for Figs. 7b and 8b, the top curve in each of these panels corresponds to noise with amplitude $\eta = 10^{-7.5}$ which, once again, is the weakest noise not to occasion a significant increase in the overall efficacy of chaotic mixing.

VI. TRANSITIONS BETWEEN 'REGULAR' AND 'CHAOTIC' BEHAVIOUR

Friction and noise can convert regular orbits into chaotic orbits and vice versa. Suppose, *e.g.,* that an initially chaotic orbit is evolved in a smooth potential in the presence of noise for some finite period and that the noise is then turned off. If the evolution is continued in the absence of noise, one may then find that the orbit has become regular with no positive Lyapunov exponents. Why this can happen is easy to understand: Noise serves to continually 'bump' the orbit from one smooth characteristic to another and it is quite possible that such 'bumps' will eventually deflect the orbit from a chaotic to a regular characteristic. To the extent that discreteness effects can be mimicked by noise, one would anticipate similar transitions in an N-body evolution [28].

This was not an issue for orbits evolved in the potentials (3.2) and (3.5), both of which are integrable. This possibility is also unimportant for the nonintegrable black hole plus ellipsoid potential discussed above since, for the energies and black hole masses that were considered, the energetically accessible phase space is almost completely chaotic. However, the possibility of such transitions is a major issue for the Dehnen potential where, for most energies, the constant energy hypersurface admits large measures of both regular and chaotic orbits.

A hint that such transitions may be present derives from a computation of Dr, the mean separation between frozen-N orbits and smooth characteristics with the same initial condition, generated from ensembles of initial conditions corresponding to only regular or only chaotic orbits. One example is provided in Fig. 13, which exhibits $Dr(t)$ for ensembles evolved in frozen-N realisations of the Dehnen distribution with $N = 10^4$, $N = 10^{4.5}$, and $N = 10^5$. The three left panels were generated from regular initial conditions; the three right panels from chaotic initial conditions. Both sets of initial conditions were selected to have very low energies, so that they were restricted to the central portions of the system [27].

It is clear that the chaotic initial conditions yield a more 'irregular' time dependence although, as expected, in both cases Dr evidences a nearly linear growth in time. However, it is also obvious that the growth time t_G for the chaotic initial conditions is *not* much longer than the growth time for the regular initial conditions. For all three values of N, the best fit value of t_G is comparable for the regular and chaotic initial conditions although, for $N = 10^5$, it is clear that Dr grows somewhat more slowly for the regular orbits. The obvious interpretation is that, even at very early times, a significant fraction of the initial conditions have switched between 'regular' and 'chaotic' behaviour.

Direct proof that such transitions occur, and an estimate of the transition time scale, is straightforward to obtain. Given orbital data from frozen-N ensembles integrated for a total time T, one can use snapshots at earlier times $\tau < T$ to generate new ensembles of initial conditions and integrate those ensembles in the smooth potential to compute Lyapunov exponents. Comparing the results of such integrations with integrations of the original initial conditions in the smooth potential then permits one to quantify the extent to which discreteness effects have made a regular ensemble 'less regular' and/or a chaotic ensemble 'less chaotic.' [29]

The results of such an analysis are summarised in Fig. 14, which plots the mean finite time Lyapunov exponent $\langle \chi_S \rangle$ for smooth orbit ensembles as a function of τ. The three left panels were generated for the low energy ensembles; the three right panels for the high energy panels. In each case the initially chaotic ensembles are represented by diamonds and a solid line; the initially regular ensembles are represented by triangles and a dashed line. The three rows again correspond, respectively, to $N = 10^4$, $N = 10^{4.5}$, and $N = 10^5$.

In each case the mean χ_S for the initially chaotic ensembles decreases systematically with τ and the mean χ_S for the regular ensembles increases, exactly what would be expected if, as τ increases, progressively larger numbers of transitions between regularity and chaos have occured during the frozen-N evolution. Indeed, to the extent that the two ensembles of initial conditions sample the same phase space regions, one would expect that the values of χ_S for the regular and chaotic ensembles should converge to a common value. It is evident that, for the lower energy ensemble, convergence or near-convergence has in fact been achieved for the largest values of τ, and it is also apparent that convergence happens more rapidly for smaller N. This again is exactly as expected. Larger N corresponds to weaker 'noise,' but weaker noise should be less effective in inducing transitions.

A priori it might seem surprising that the mean χ_S for the regular orbits approaches its limiting value much more quickly than does the mean for the chaotic orbits. This, however, is likely a manifestation of the phase space structure associated with the Dehnen potential. For both low and high energies, the initially regular ensemble corresponds in the smooth potential to box orbits which occasionally pass quite close to the center of the system; but, in the center, the regular and chaotic phase space regions are entangled in a very complex fashion, so that it is comparatively simple for initially regular orbits to be deflected to chaotic trajectories.

VII. DISCUSSION

The experiments described in this paper lead to several unambiguous conclusions regarding the behaviour of orbits and orbit ensembles evolved in frozen-N realisations of smooth density distributions.

It is, for example, clear that ordinary Lyapunov exponents computed for individual frozen-N trajectories do *not* provide a useful characterisation of the degree of *macroscopic chaos* manifested by these trajectories. Different initial conditions with the same energy evolved in frozen-N realisations of a specified potential typically have Lyapunov exponents that are comparable in magnitude and exhibit little if any dependence on N, even though, in terms of their bulk properties, one may look very nearly regular and another wildly chaotic.

This can be interpreted by asserting that, at least for large N, one can make comparatively clear distinctions between two types of chaos which may be associated with the N-body problem. On the one hand, there is *microscopic chaos* associated with close encounters between nearby masses. This chaos, which is presumably responsible for the large Lyapunov exponents associated with frozen-N orbits, is (almost) always present but, at least for comparatively large N, tends to 'wash out' macroscopically. On the other hand, there may be *macroscopic chaos* which, if present in the continuum limit, will also have manifestations in frozen-N simulations.

The experiments also demonstrate a clear sense in which, as N increases, frozen-N trajectories become 'more similar' to smooth potential characteristics generate from the same initial condition. In particular, it becomes progressively easier to distinguish between 'regular' and 'chaotic' macroscopic behaviour. This similarity can be quantified in at least three different ways:

1. *The rate at which frozen-N orbits and smooth characteristics diverge.* For both regular and chaotic initial conditions, frozen-N trajectories and smooth characteristics tend to diverge linearly in time. However, the N-dependence of the time scale t_G associated with this divergence differs dramatically. For initial conditions corresponding to regular orbits, $t_G \propto N^{1/2}$; for chaotic initial conditions, $t_G \propto \ln N$. It follows that, for large N, frozen-N trajectories and smooth characteristics corresponding to regular orbits remain 'close' much longer than do trajectories and characteristics corresponding to chaotic orbits.
2. *The 'complexity' of Fourier spectra constructed from orbital time series.* For small N, both regular and chaotic initial conditions will, when integrated into the future, yield Fourier spectra that are much more complex than the spectra associated with an evolution in the smooth potential. In particular, both regular and chaotic orbits will yield spectra of comparable complexity. However, as N increases the complexities decrease and, for sufficiently large N, one sees a convergence towards the complexities appropriate for smooth characteristics with the same ini-

tial conditions, be these either regular or chaotic.
3. *The bulk properties of phase mixing, as probed,* e.g. *by lower order moments.* Phase mixing of initially localised ensembles in frozen-N systems is invariably more efficient than phase mixing in the corresponding smooth potential but, as N increases, the observed evolution comes to more closely resemble phase mixing of the same initial conditions evolved in the smooth potential.

At least for comparatively large N, many discreteness effects can be well mimicked by energy-conserving white noise with amplitude $\eta \propto 1/N$. This is in close agreement with naive expectations based on the modeling of discreteness effects as a sequence of incoherent binary encounters, which would suggest $\eta \propto (\ln N)/N$; and indeed, the simulations are also consistent with the latter dependence. Modeling discreteness effects in terms of noise works well in predicting both the expected complexities of individual frozen-N trajectories and moments associated with phase mixing. This indicates that, at least for large N, *noise can be used to model both bulk statistical properties of orbit ensembles* and *qualitative properties of individual orbits.* This suggests strongly that investigations of the effects of white noise on orbits in nonintegrable potentials – which are much less expensive computationally than frozen-N integrations – can provide information about the effects of graininess.

That noise really can mimic the effects of graininess is nontrivial theoretically. The notion that discreteness effects can be modelled using friction and white noise is based on calculations [3,4] of bulk properties of orbits over very long time scales $t_R \sim (N/\ln N)t_D$, and involved the tacit assumption that the flow is regular. The effects explored in this paper focus on time scales $\ll t_R$, consider also the behaviour of individual orbits, and incorporate explicitly the possibility of macroscopic chaos.

Nevertheless, it is clear that modeling discreteness effects by white noise is *not* completely satisfactory. The agreement between frozen-N and noisy integrations is poor for comparatively small N; and noisy integrations of the form described in this paper cannot be used to obtain estimates of the Lyapunov exponents associated with frozen-N orbits. The development of a 'more realistic' noise and its use to model systems with $N \gg 10^5$ is currently underway.

Discreteness effects can induce transitions between different orbit 'types,' including both transitions between regular and chaotic behaviour, which are impossible in the smooth potential, and transitions between (say) 'sticky' and 'wildly chaotic' behaviour which, in the smooth potential, is not forbidden but typically occurs only on a much longer time scale. Not surprisingly these transitions appear to be more common for smaller N. Indeed, the simulations are consistent with the interpretation that, for sufficiently large N, transitions between regular and chaos become essentially impossible and transitions between sticky and wildly chaotic behaviour happen no more quickly than in the continuum limit.

Finally, and perhaps most importantly, it appears that, at least in terms of macroscopic properties, *it does make sense to speak of a smooth $N \to \infty$ continuum limit. However, convergence towards this limit is much slower for density distributions which, in the continuum limit, correspond to nonintegrable potentials that admit chaotic orbits.*

ACKNOWLEDGMENTS

It is a pleasure to acknowledge useful discussions with Court Bohn, Ilya Pogorelov, and Christos Siopis. Partial financial support was provided by NSF AST-0070809. The computations involving orbital ensembles in the Dehnen potential were performed using resources of the National Energy Research Scientific Computing Center, which is supported by the Office of Science of the U.S. Department of Energy under Contract No. DE-AC03-76SF00098.

[1] H. E. Kandrup and I. V. Sideris, Phys. Rev. **E 64**, 056209 (2002).
[2] M. Valluri and D. Merritt, in *The Chaotic Universe*, edited by R. Ruffini and V. G. Gurzadyan (World Scientific, New York, 1999).
[3] S. Chandrasekhar, Rev. Mod. Phys. **15**, 1 (1943).
[4] S. Chandrasekgar, *Principles of Stellar Dynamics* (University of Chicago, Chicago, 1943). See also M. N. Rosenbluth, W. M. MacDonald, and D. L. Judd, Phys. Rev. **107**, 1 (1957) for analogous computations for a plasma.
[5] S. Habib, H. E. Kandrup, and M. E. Mahon, Astrophys. J. *480*, 155 (1997).
[6] H. E. Kandrup, B. L. Eckstein, and B. O. Bradley, Astron. Astrophys. **320**, 65 (1997).
[7] M. Tabor, *Chaos and Integrability in Nonlinear Dynamics* (Wiley, New York, 1989).
[8] M. E. Mahon *et al*, Mon. Not. R. astr. Soc. *275*, 443 (1995).
[9] H. E. Kandrup, Mon. Not. R. astr. Soc. **301**, 960 (1998).
[10] I. V. Pogorelov and H. E. Kandrup, Phys. Rev. **E 60**, 1567 (1999).
[11] R. A. Kishek *et al*, *Proceedings of the 2001 IEEE Particle Accelerator Conference in Chicago* (IEEE Press, New York, in press).
[12] C. L. Bohn, H. E. Kandrup, and R. A. Kishek, *Proceedings of Snowmass 2001*, in press.
[13] The paper by D. Merritt and Valluri, Astrophys. J. **471**, 82 (1996) entailed an extension to three dimensions of ideas introduced in H. E. Kandrup and M. E. Mahon, *Phys. Rev.* **E 49**, 3735 (1994) in the context of a simple two-dimensional model, namely the sixth order truncation of the Toda lattice potential.

[14] *Cf.* G. Bertin, *Dynamics of Galaxies* (Cambridge University Press, Cambridge, 2000)
[15] H. E. Kandrup and I. V. Sideris, Celestial Mechanics **82**, 61 (2001).
[16] W. Dehnen, Mon. Not. R. astr. Soc. **265**, 250 (1993).
[17] D. Merritt and T. Fridman, Astrophys. J. **460**, 136 (1996)
[18] C. Siopis and H. E. Kandrup, Mon. Not. R. astr. Soc. **319**, 43 (2000)
[19] C. Siopis, Ph. D. University of Florida, dissertation, 1998..
[20] *Cf.* A. J. Lichtenberg and M. A. Lieberman, *Regular and Chaotic Dynamics* (Springer, Berlin, 1992).
[21] N. G. van Kampen, *Stochastic Processes in Physics and Chemistry* (North Holland, Amsterdam, 1981).
[22] A. Griner, W. Strittmatter, and J. Honerkamp, J. Stat. Phys. *51*, 95 (1989).
[23] Following, G. Contopoulos, Astron. J. **76**, 147 (1971), the term 'sticky' is used here to designate segments of chaotic orbits which, because of topological obstructions like cantori, are trapped temporarily near regular phase space regions. Such 'sticky' orbit segments typically have finite time Lyapunov exponents that are considerably smaller than those associated with unsticky, wildly chaotic segments; and they tend to be 'more regular' in visual appearance, characterised by considerably lower complexities [6]. Visual examples of 'stickiness' are given in Fig. 1 in [10].
[24] These ensembles sampled Merritt and Fridman's [17] 'shell' 8, for which, in the continuum limit, $E \approx -0.4478$.
[25] Modulo the case of a constant density sphere, where evey unperturbed orbit has the same unperturbed frequencies, so that linear phase mixing is impossible.
[26] *Cf.* Fig. 9 in C. Siopis, B. L. Eckstein, and H. E. Kandrup, Ann N. Y. Acad. Sci. **867**, 41 (1998).
[27] The ensembles sampled the lowest energy 'shell' considered by Merritt and Fridman [17], for which $E \approx -0.9964$.
[28] C. L. Bohn and J. R. Delayen, Phys. Rev. **E 50**, 1516 (1994).
[29] One might, naively, suppose that the relative number of regular and chaotic orbits in each ensemble would provide a more satisfactory probe. However, as discussed in [18], 'stickiness' is so pronounced in the Dehnen potential that integrations for times as short as $t = 10^3 - 10^4$ are not always sufficient to make sharp distinctions between regularity and chaos. For the lower energy orbits, χ_S was computed by integrating for a time $T = 256$; for the higher energy, $T = 1024$.

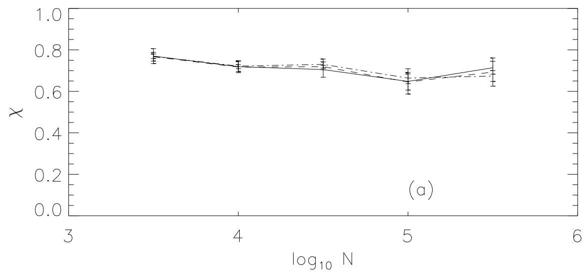

FIG. 1. Estimates of the largest Lyapunov exponent for orbits evolved in frozen-N realisations of a homogeneous ellipsoid: integrable initial conditions evolved with $M_{BH} = 0$ (solid line), 'sticky' initial conditions evolved with $M_{BH} = 10^{-1.5}$ (dashed line), and 'wildly chaotic' initial conditions with $M_{BH} = 10^{-1.5}$ (dot-dashed line).

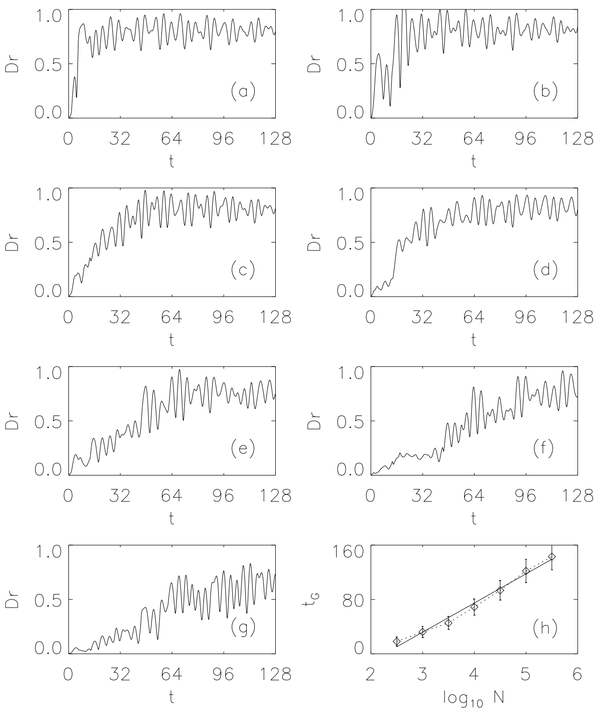

FIG. 2. The mean separation, $\mathcal{D}r$, between frozen-N orbits and smooth characteristics with the same initial conditions, computed for ensembles of 800 chaotic initial conditions evolved in the potential (3.6) for variable N. (a) $N = 10^{2.5}$. (b) $N = 10^3$. (c) $N = 10^{3.5}$. (d) $N = 10^4$. (e) $N = 10^{4.5}$. (f) $N = 10^5$. (g) $N = 10^{5.5}$. (h) The growth rate $t_G(N)$ extracted from the preceding panels, assuming a linear growth law. The solid line overlays a least squares fit $t_G = A + B \log_{10} N$.

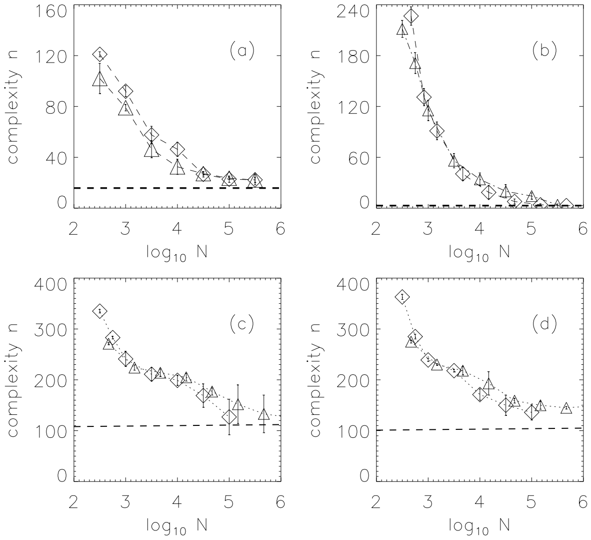

FIG. 3. The mean complexity n for orbits evolved in the potentials (3.2), (3.5), and (3.6), considering both frozen-N orbits with variable N (diamonds) and smooth orbits perturbed by noise with $\Theta = 1.0$ and variable η (triangles). η was related to N by the relation $\eta = e^{\mathcal{A}}/N$, with $\mathcal{A}$ determined as described in the text. The dashed horizontal line exhibits the mean complexity of orbits with the same initial conditions evolved in the smooth potential in the absence of noise. (a) Regular orbits in the Plummer potential. (b) Regular orbits in the homogeneous ellipsoid potential. (c) Wildly chaotic orbits in the ellipsoid plus black hole potential. (d) 'Sticky' chaotic orbits in the ellipsoid plus black hole potential.

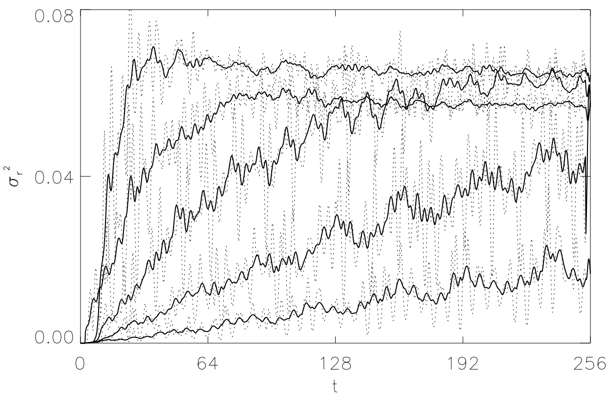

FIG. 4. σ_r^2, the square of the configuration dispersion associated with an initially localised ensemble evolved in frozen-N realisations of the integrable ellipsoid potential (3.5) with (from top to bottom) $N = 10^3$, $N = 10^{3.5}$, $N = 10^4$, $N = 10^{4.5}$, and $N = 10^5$.

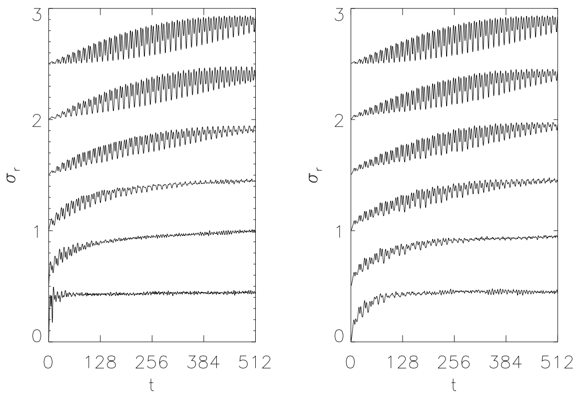

FIG. 5. (a) The configuration dispersion σ_r associated with an initially localised ensemble evolved in frozen-N realisations of the integrable Plummer potential (3.2) for (from bottom to top) $N = 10^3$, $N = 10^{3.5}$, $N = 10^4$, $N = 10^{4.5}$, and $N = 10^5$. The top curve represents unperturbed evolution in the smooth potential. Successive curves are staggered upwards by distances $\sigma = 0.5$. (b) σ_r for the same initial conditions evolved in the smooth potential, but perturbed by energy-conserving white noise with $\Theta = 1.0$ and $\eta = 10^{-3}$, $\eta = 10^{-3.5}$, $\eta = 10^{-4}$, $\eta = 10^{-4.5}$, $\eta = 10^{-5}$, and $\eta = 10^{-5.5}$.

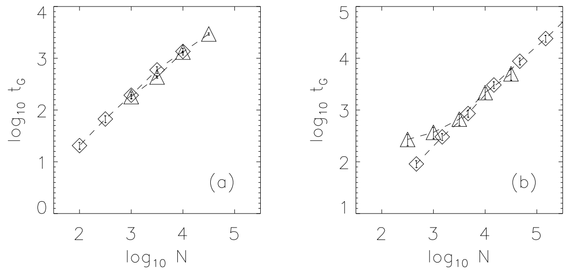

FIG. 6. (a) The growth time $t_G(N)$ for the dispersion σ_r for orbit ensembles evolved in frozen-N realisations of the Plummer potential (diamonds) and the corresponding growth time $t_G(\eta)$ for orbit ensembles evolved in the smooth Plummer potential in the presence of energy-conserving white noise with $\Theta = 1.0$ and $\log_{10}\eta = -\log_{10} N$ (triangles). (b) $t_G(N)$ and $t_G(\eta)$ for orbit ensembles in the homogeneous ellipsoid potential, now setting $\log_{10}\eta = -\log_{10} N + 0.6$.

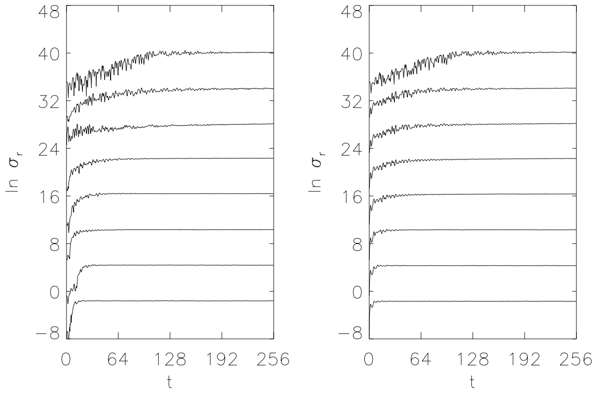

FIG. 7. (a) The configuration dispersion σ_r associated with an initially localised ensemble of wildly chaotic orbits evolved in frozen-N realisations of the nonintegrable potential (3.6) with (from bottom to top) $N = 10^{2.5}$, $N = 10^3$, $N = 10^{3.5}$, $N = 10^4$, $N = 10^{4.5}$, $N = 10^5$, and $N = 10^{5.5}$. The top curve represents unperturbed evolution in the smooth potential. (b) σ_r for the same ensemble, now evolved in the presence of noise with $\Theta = 1.0$ and $\eta = 10^{-2}$, $\eta = 10^{-2.5}$, $\eta = 10^{-3}$, $\eta = 10^{-3.5}$, $\eta = 10^{-4}$, $\eta = 10^{-4.5}$, $\eta = 10^{-5}$, and $\eta = 10^{-7.5}$.

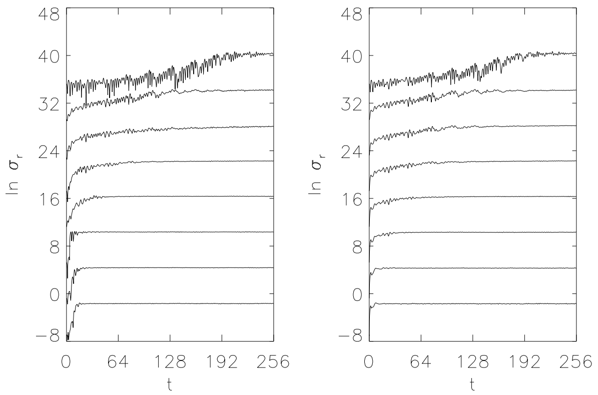

FIG. 8. (a) The configuration dispersion σ_r associated with an initially localised ensemble of 'sticky' chaotic orbits evolved in frozen-N realisations of the nonintegrable potential (3.6) with (from bottom to top) $N = 10^{2.5}$, $N = 10^3$, $N = 10^{3.5}$, $N = 10^4$, $N = 10^{4.5}$, $N = 10^5$, and $N = 10^{5.5}$. The top curve represents unperturbed evolution in the smooth potential. (b) σ_r for the same ensemble, now evolved in the presence of noise with $\Theta = 1.0$ and $\eta = 10^{-2}$, $\eta = 10^{-2.5}$, $\eta = 10^{-3}$, $\eta = 10^{-3.5}$, $\eta = 10^{-4}$, $\eta = 10^{-4.5}$, $\eta = 10^{-5}$, and $\eta = 10^{-7.5}$.

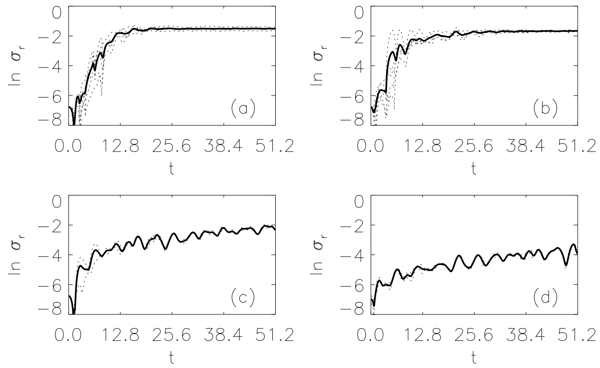

FIG. 9. The configuration dispersion σ_r associated with the ensemble exhibited in the preceding Figure, now restricted to a shorter time interval. The thick solid line represents an average over different runs corresponding to the lighter curves. (a) $N = 10^{2.5}$. (b) $N = 10^{3.5}$. (c) $N = 10^{4.5}$. (d) $N = 10^{5.5}$.

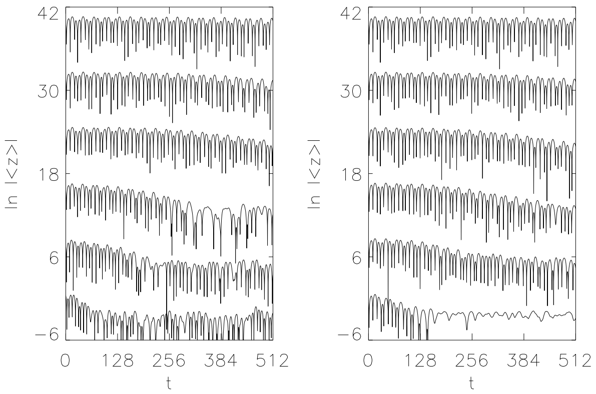

FIG. 10. (a) The quantity $\ln |\langle z \rangle|$ for an initially localised ensemble evolved in frozen-N realisations of the integrable Plummer potential (3.2) with (from bottom to top) $N = 10^3$. $N = 10^{3.5}$, $N = 10^4$, $N = 10^{4.5}$, and $N = 10^5$. The top curve corresponds to evootion in the smooth potential. (b) $\ln |\langle z \rangle|$ computed for the same initial conditions, now evolved in the smooth potential in the presence of energy-conserving noise with $\eta = 10^{-3}$, $\eta = 10^{-3.5}$, $\eta = 10^{-4}$, $\eta = 10^{-4.5}$, $\eta = 10^{-5}$, and $\eta = 10^{-5.5}$.

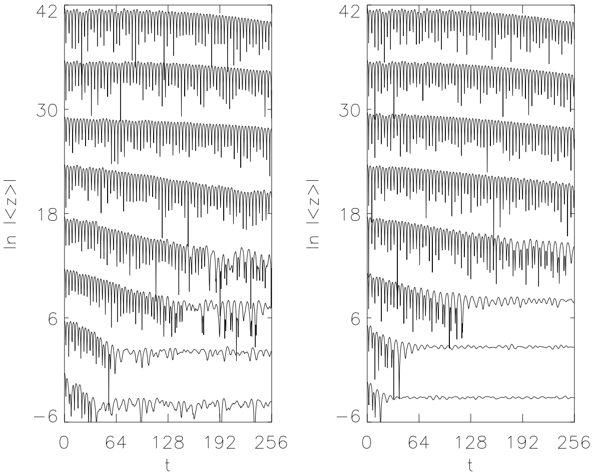

FIG. 11. (a) The quantity $\ln|\langle z\rangle|$ for an initially localised ensemble of wildly chaotic orbits evolved in frozen-N realisations of the nonintegrable potential (3.6) with (from bottom to top) $N = 10^{2.5}$, $N = 10^3$, $N = 10^{3.5}$, $N = 10^4$, $N = 10^{4.5}$, $N = 10^5$ and $N = 10^{5.5}$. The top curve corresponds to evolution in the smooth potential. (b) $\ln|\langle z\rangle|$ computed for the same initial conditions, now evolved in the smooth potential in the presence of energy-conserving noise with $\eta = 10^{-2}$, $\eta = 10^{-2.5}$, $\eta = 10^{-3}$, $\eta = 10^{-3.5}$, $\eta = 10^{-4}$, $\eta = 10^{-4.5}$, $\eta = 10^{-5}$, and $\eta = 10^{-7.5}$.

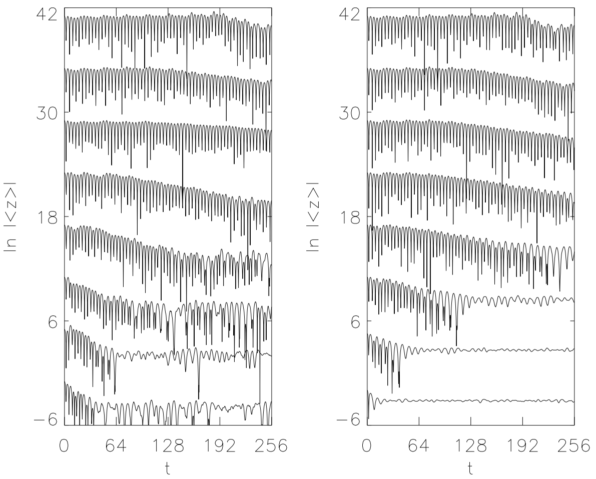

FIG. 12. (a) The quantity $\ln|\langle z\rangle|$ for an initially localised ensemble of 'sticky' chaotic orbits evolved in frozen-N realisations of the nonintegrable potential (3.6) with (from bottom to top) $N = 10^{2.5}$, $N = 10^3$, $N = 10^{3.5}$, $N = 10^4$, $N = 10^{4.5}$, $N = 10^5$ and $N = 10^{5.5}$. The top curve corresponds to evolution in the smooth potential. (b) $\ln|\langle z\rangle|$ computed for the same initial conditions, now evolved in the smooth potential in the presence of energy-conserving noise with $\eta = 10^{-2}$, $\eta = 10^{-2.5}$, $\eta = 10^{-3}$, $\eta = 10^{-3.5}$, $\eta = 10^{-4}$, $\eta = 10^{-4.5}$, $\eta = 10^{-5}$, and $\eta = 10^{-7.5}$.

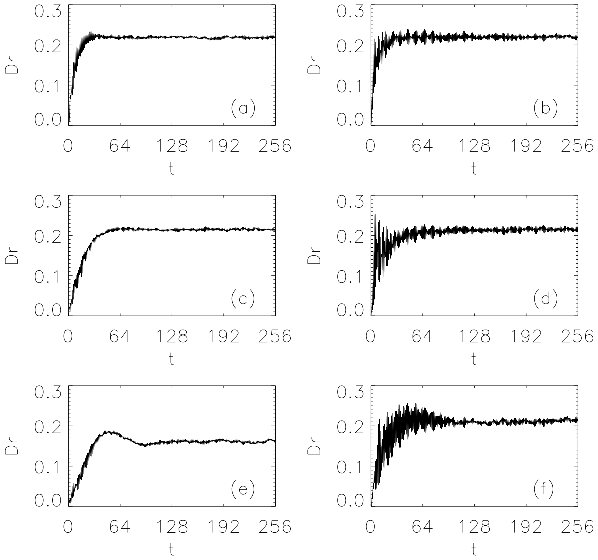

FIG. 13. The quantity $\mathcal{D}r$ for two different initially localised ensembles of 'sticky' chaotic orbits with the same (low) energies, each evolved in frozen-N realisations of the Dehnen potential. (a) A 'regular' ensemble with $N = 10^4$. (b) A 'chaotic' ensemble with $N = 10^4$. (c) The 'regular' ensemble with $N = 10^{4.5}$. (d) The 'chaotic' ensemble with $N = 10^{4.5}$. (e) The 'regular' ensemble with $N = 10^5$. (f) The 'chaotic' ensemble with $N = 10^5$.

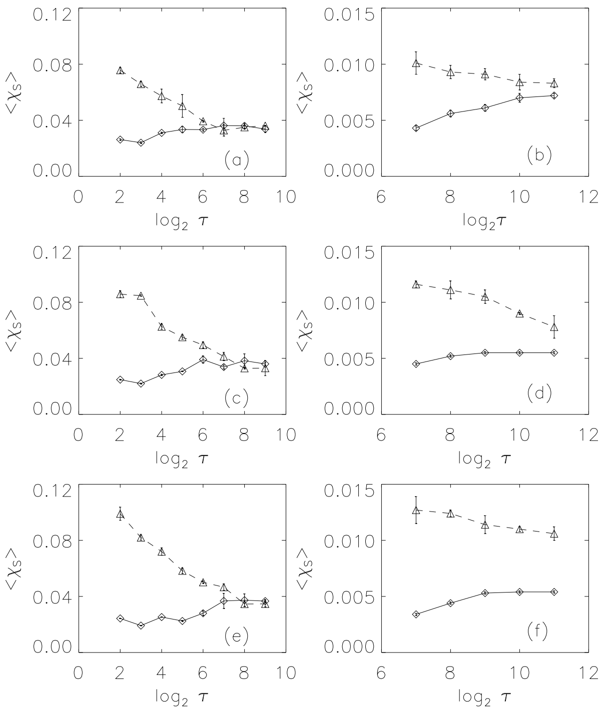

FIG. 14. The mean Lyapunov exponent $\langle\chi_S\rangle$, for ensembles evolved in the smooth Dehnen potential, selecting as initial conditions the final phase space coordinates of orbits that had been evolved in frozen-N potentials for some time τ. (a) Initially regular (solid line) and chaotic (dashed line) low energy orbits evolved with $N = 10^4$. (b) Initially regular (solid line) and chaotic (dashed line) higher energy orbits evolved with $N = 10^4$. (c) The same as (a) but for $N = 10^{4.5}$. (d) The same as (b) but for $N = 10^{4.5}$. (e) The same as (a) but for $N = 10^5$. (f) The same as (b) but for $N = 10^5$.